

HOSTED BY



ELSEVIER

Contents lists available at ScienceDirect

Atmospheric Pollution Research

journal homepage: www.elsevier.com/locate/aprRegional HYSPLIT simulation of atmospheric transport and deposition of the Chernobyl ^{137}Cs releasesOleg Skrynyk^{a,*}, Volodymyr Voloshchuk^a, Igor Budak^a, Sergiy Bubin^b^a Ukrainian Hydrometeorological Institute, Kyiv, Ukraine^b Department of Physics, Nazarbayev University, Nur-Sultan, Kazakhstan

ARTICLE INFO

Keywords:

HYSPLIT

Chernobyl accident

Wet and dry removals

 ^{137}Cs depositions

CALPUFF

ABSTRACT

In this work we report the results of HYSPLIT numerical simulations of the Chernobyl ^{137}Cs atmospheric transport, dispersion, and deposition on the regional scale (~1000 km from the source) with the main focus on the analysis of the deposition processes. In the simulations we used three different gridded datasets of input meteorology and three release scenarios previously published in the literature. The resistance method and the predefined constant value of the deposition velocity (0.005 m/s) were applied to calculate dry depositions whereas an approach based on a scavenging coefficient was used for both wet in-cloud and below-cloud removals. The results were statistically evaluated against the measurements of ^{137}Cs total depositions on the territory of Ukraine. Our simulations show considerable dependence of the HYSPLIT-predicted accumulated deposition pattern on both the input meteorology and source parameterizations. The best performance of HYSPLIT was obtained with the ERA Interim reanalysis data and the source model of Talerko (2005) and the constant deposition velocity. This simulation reproduced fairly well the spatial structure of the ^{137}Cs contamination on the territory of Ukraine with good evaluation statistics. However, not all significant local maxima of the contamination pattern were captured clearly. Our simulations also show that dry removal processes account for approximately 50% of the total depositions in Ukraine. Both wet in-cloud and below-cloud removal mechanisms had roughly equal influence on the total amount of ^{137}Cs radionuclides deposited on the territory of Ukraine.

1. Introduction

Modeling the atmospheric transport, dispersion and deposition of radioactive materials released in April/May 1986 from the destroyed core of the Chernobyl nuclear power plant (NPP) has been subject of many recent studies (e.g. Evangelidou et al., 2013; Simsek et al., 2014; Evangelidou et al., 2016; Evangelidou et al., 2017; Giaiotti et al., 2018). The Chernobyl catastrophe along with the Fukushima Daiichi nuclear disaster are the two largest accidents on NPPs. Both caused significant radioactive contamination of large territories. Multiple studies have aimed to reproduce (through numerical simulation) the physical processes determining the fate of the emitted radioactive pollutants on the regional and global scale (e.g. Pudykiewicz, 1988; Klug et al., 1992; Baklanov and Sørensen, 2001; Brandt et al., 2002; Talerko, 2005; Masson et al., 2011; Stohl et al., 2012; Kovalets et al., 2014; Leadbetter et al., 2015). Yet the simulations results reported in these studies

(pollutant air concentrations and wet and dry deposition fluxes to the ground) still contain many uncertainties (e.g. Kajino et al., 2018). The prime cause of these uncertainties seems to originate from insufficiently accurate input information regarding emitting source characteristics (e.g. Sugiyama et al., 2012; Evangelidou et al., 2017; Geng et al., 2017). However, the input meteorology (e.g. Draxler et al., 2013; Arnold et al., 2015; Leadbetter et al., 2015) and dispersion models (e.g. Draxler et al., 2013; Leadbetter et al., 2015; Giaiotti et al., 2018) also contribute to the discrepancy between the calculated results and measurements (Leelőssy et al., 2018).

The main objective of this work has been to simulate atmospheric transport, dispersion and deposition of the Chernobyl radioactive Cesium (^{137}Cs) on the regional scale (~1000 km from the source) using the well-known dispersion model HYSPLIT (Draxler and Hess, 1998; Draxler, 1999; Stein et al., 2015). We aimed to achieve deeper understanding of the physical conditions, processes, and mechanisms

Peer review under responsibility of Turkish National Committee for Air Pollution Research and Control.

* Corresponding author.

E-mail addresses: skrynyk@uhmi.org.ua (O. Skrynyk), v_voloshchuk@uhmi.org.ua (V. Voloshchuk), igorvb@mail.ua (I. Budak), sergiy.bubin@nu.edu.kz (S. Bubin).<https://doi.org/10.1016/j.apr.2019.09.001>

Received 1 March 2019; Received in revised form 24 August 2019; Accepted 4 September 2019

Available online 06 September 2019

1309-1042/ © 2019 Turkish National Committee for Air Pollution Research and Control. Production and hosting by Elsevier B.V. All rights reserved.

responsible for the creation of the extremely complicated deposition pattern on the territory of Ukraine that features strong contamination spatial variability (De Cort et al., 1998). Our focus was put mainly on rather rough separation between dry and wet removal mechanisms.

Some simulations of the Chernobyl ^{137}Cs releases using HYSPLIT has been already done by other authors (Draxler and Hess, 1998; Kinser, 2001). In (Draxler and Hess, 1998) the CNPP accidental ^{137}Cs releases were simulated and used for demonstrating the applicability of HYSPLIT to model deposition processes. The study modeled only the emissions during the first day of the catastrophe over the northern part of Europe and the deposition calculations were compared to available measurements. In addition to the calculation of the total depositions, relative influence of different types of deposition processes (dry, wet in-cloud, wet below-cloud) was also studied. According to the conclusions of that work, wet deposition processes played a key role in the formation of contamination (dry removal accounted only for $\sim 1/3$ of the total deposition) with significant domination of the in-cloud removal processes.

In (Kinser, 2001) the main focus was made on wet deposition of ^{137}Cs on the European territory (continental scale). The main objective of the work was to propose some improvements to HYSPLIT's calculating scheme for the in-cloud wet scavenging processes. The results (deposition fluxes) obtained with the modified parameterization of wet deposition calculations were compared against measurements (extracted from the REM (Radioactivity Environmental Monitoring) database (JRC, 2019)) in a rather limited number of sampling sites located mainly in Western European countries such as Austria and Germany. The comparison was made for both daily and cumulative depositions. Unfortunately, the measurements of ^{137}Cs cumulative depositions from the former USSR (including Ukraine) were not available for evaluation purposes in that study. The proposed modification to HYSPLIT's wet deposition parameterization yielded no conclusive evidence of either a better or worse performance of the model. The main reasons for such a conclusion are likely to be the large uncertainty of the accidental release (which did not allow for conducting consistent and accurate simulations) and sparse evaluation data (which did not allow for obtaining a reliable assessment of the results).

Since the time the above two works were published, more detailed and accurate parameterizations of the Chernobyl source term have been proposed (e.g. Brandt et al., 2002; Talerko, 2005; Evangelou et al., 2017). Also, many features of the HYSPLIT model have been improved and updated, and new features have been added (Stein et al., 2015). Lastly, more detailed and accurate databases of gridded meteorology have been developed (e.g. Dee et al., 2011) and the capabilities of applying prognostic models in order to obtain detailed meteorological input data for dispersion modeling have increased considerably. This all makes it interesting to reexamine the results by performing HYSPLIT simulations with newly available information. In the present work, which we plan to be the first in a series, we focus our attention on the regional scale. The simulation of the Chernobyl ^{137}Cs fallout on the European (continental) scale will be the subject of future works.

It is worth noting that besides works (Draxler and Hess, 1998; Kinser, 2001) HYSPLIT has been used in a number of studies of the atmospheric transport, dispersion, and deposition of different pollutants (see e.g. Stein et al. (2015) and references therein), including radioactive materials released from other accidents (e.g. Kinoshita et al., 2011; Draxler and Rolph, 2012; Draxler et al., 2013; Katata et al., 2015) or nuclear weapons tests (Moroz et al., 2010; Rolph et al., 2014). The simulations have demonstrated a fairly good performance of the HYSPLIT model.

2. Materials and methods

2.1. HYSPLIT model and configuration of simulations

The National Oceanic and Atmospheric Administration (NOAA) Air

Resources Laboratory's (ARL) HYSPLIT model is a complete system for computing simple particle (indivisible air parcel) trajectories as well as transport, dispersion, chemical transformation, and deposition simulations under complex (time- and space-varying) meteorological driving forces (Draxler and Hess, 1998; Draxler, 1999; Stein et al., 2015). HYSPLIT performs calculations based on gridded meteorological data that must be prepared separately. To calculate pollutant dispersion, the model can be configured to use either a 3-D particle mode or a puff mode. A hybrid scheme (particles in vertical direction and puffs horizontally) can also be used. In our simulations we applied the 3D particle modeling approach, which is recommended in (HYSPLIT, 2018). However, the Gaussian puff representation of pollutant emissions was also used in our work in order to make a reliable comparison with the pure puff model, CALPUFF, that was previously used to simulate the Chernobyl ^{137}Cs release on the same domain (Gaiotti et al., 2018).

In the 3D particle computational mode, 10 000 particles were released every emission cycle. We determined that such number of released particles was an optimal balance between the computational cost and accuracy. It was checked based on the sensitivity tests with increasing number of released particles. The results (min and max air concentration) obtained with 1000 and 10000 particles differed by less than 5%. Other control parameters of the model were taken equal to the default values.

The computational domain (Fig. 1) covers the territory of Ukraine and the nearest parts of its neighboring countries expanding over 20° in longitude (from West to East) and 10° in latitude (from South to North) directions respectively with the center at (49.00°N, 31.50°E) and the spatial resolution of the computational grid of 0.15° (~ 15 km).

The output concentration field on the domain was calculated over a vertical layer with 100 m in depth.

In our work we paid close attention to the deposition processes. A brief summary about both wet and dry removal calculation schemes used in HYSPLIT is provided below according to (Draxler and Hess, 2017; HYSPLIT, 2018). Wet and dry removal processes of aerosol particles are parameterized through exponential removal constants. That is, the total deposited pollutant mass, D , over time step, Δt , is calculated using the formula

$$D = m \{1 - \exp[-\Delta t (\beta_{dry} + \beta_{inc} + \beta_{bel})]\}, \quad (1)$$

where m is the pollutant mass of either a particle or a puff, while β_{dry} , β_{inc} , β_{bel} are the inverse time constants for dry removal, in-cloud wet removal, and below-cloud wet removal respectively. The pollutant mass is then reduced by the deposition amount given by expression (1).

The dry deposition constant β_{dry} is defined as

$$\beta_{dry} = v_d \Delta Z_{sfc}^{-1},$$

where v_d is the deposition velocity, and ΔZ_{sfc} is the depth of the surface layer (usually defined internally to the model as the second meteorological data level). Pollutants are dry deposited only if they are within the surface layer. The deposition velocity for particular matter in HYSPLIT may be computed using the resistance method or may be assumed to be equivalent to the gravitational settling velocity (Draxler and Hess, 2017; HYSPLIT, 2018), which is defined based on the particle diameter, density, and shape parameter. However, an explicit definition of constant v_d is also allowed. In our calculations we used two approaches: the resistance method and a predefined constant value. The full resistance model appears to be the most consistent with reality as it takes into account many fine details of dry removal process, such as its time and space inhomogeneity, dependence on particle properties, turbulence structure etc.

In the current version of HYSPLIT (HYSPLIT, 2018) wet deposition calculations for particles were simplified to use the same computational approach for in-cloud and below-cloud removal calculations. Both β_{inc} and β_{bel} are defined through a scavenging constant ($8 \cdot 10^{-5} \text{ s}^{-1}$) and are expressed as

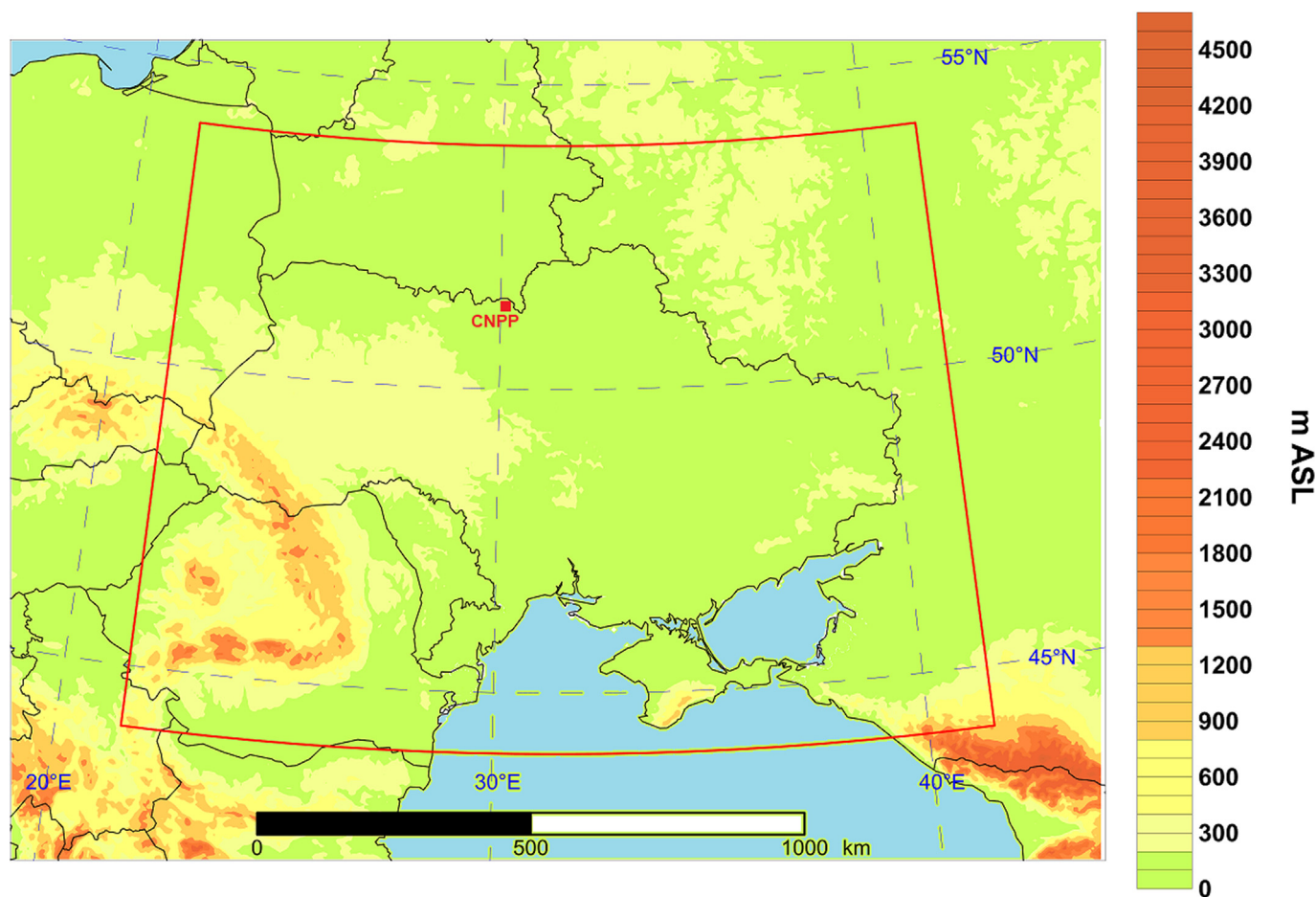


Fig. 1. HYSPLIT computational domain (inside the red frame/box) and its terrain. The location of CNPP is shown as a red dot.

$$\beta_{inc} = \beta_{bel} = 8 \cdot 10^{-5} \left(\frac{P}{P_0} \right)^{0.79},$$

where P is the precipitation rate ($[P] = mm h^{-1}$) and P_0 is reference precipitation rate ($P_0 = 1 mm h^{-1}$). According to (Draxler and Hess, 2017) in-cloud scavenging is applied to particles located within a cloud layer, whereas below-cloud scavenging is used for pollutant removal in rain below a cloud layer. The cloud bottom is defined at the level when the RH first reaches 80% and the cloud top is reached when the RH drops below 60%.

2.2. Input meteorology

In our simulations we used three different sets of gridded meteorological data which differ in spatial and temporal resolutions and methods for how they were computed. Feeding the HYSPLIT model with different input meteorology can help us understand how it can affect the simulation results. Below we provide a brief description of the datasets used.

2.2.1. NCAR/NCEP global reanalysis data

The first dataset of the input meteorology was obtained from a reanalysis conducted jointly by the National Center for Environmental Prediction (NCEP) and the National Center for Atmospheric Research (NCAR) (Kalnay et al., 1996). These global 2.5° data with time resolution of 6 h were retrieved in the ARL/HYSPLIT format from the NOAA ARL server (<http://www.ready.noaa.gov/archives.php>). The surface data provided are the surface pressure (PRSS), air temperature at 2 m (T02M), horizontal wind components at 10 m (U10M and V10M) and 6-h accumulated precipitation (TPP6). In the vertical direction 17

upper levels are defined (for every pressure level between 1000 and 10 hPa), where the values of height (HGTS), temperature (TEMP), horizontal wind components (UWND and VWND), vertical wind velocity (WWND) and relative humidity (RELH) are provided.

The spatial resolution of these data is coarse. Nevertheless, we used them in our simulations in order to compare with other results and understand how the spatial resolution of the input meteorology can vary the deposition pattern.

2.2.2. ECMWF ERA interim reanalysis data

ERA Interim reanalysis data (Dee et al., 2011) were developed by the European Center for Medium-Range Weather Forecasts (ECMWF). The data for April/May of 1986 were retrieved from the ECMWF web site (<https://www.ecmwf.int>). Their horizontal spatial resolution is 0.75° (considerably higher compared to the NCAR/NCEP dataset) while the time resolution is the same - 6 h. The surface data includes: surface height (SHGT), T02M, U10M, V10M and 12-h accumulated precipitation (TPPT). On 27 upper levels (for pressure levels between 1000 and 100 hPa) the values of HGTS, TEMP, UWND, VWND, WWND and RELH are provided.

2.2.3. WRF ARW data

The outputs of the prognostic model, WRF ARW version 3.6.1 (Skamarock and Klemp, 2008), were also used in our HYSPLIT dispersion calculations. The horizontal grid resolution in our WRF simulation was $30 \times 30 km^2$, whereas the temporal resolution of the model outputs was 1 h. 49 layers were defined in the vertical direction in order to resolve a complex vertical structure of the atmosphere during the catastrophe. The NCEP Climate Forecast System reanalysis data (Saha

et al., 2010) was used as the initial and boundary conditions. The WRF physics options included the Thompson scheme (Thompson et al., 2008) for microphysics, the Rapid Radiative Transfer Model for General Circulation Models (RRTMG) (Iacono et al., 2008) for both longwave and shortwave radiation, the Unified Noah land-surface model (Chen and Dudhia, 2001), the Yonsei University scheme (Hong et al., 2006) for PBL parameterization and the Grell-Freitas ensemble scheme (Grell and Freitas, 2014) for the cumulus option. As the surface/2D data the WRF output included the SHGT, PRSS, 1-h accumulated precipitation (TPP1), planetary boundary layer height (PBLH), friction velocity (USTR), sensible heat net flux (SHTF), T02M, U10M and V10M. At 49 upper levels (in the sigma-vertical coordinate) the following variables were specified and calculated: PRES, TEMP, UWND, VWND, WWND, and specific humidity (SPHU).

2.3. Emission data

Three different parameterizations of the vertical and temporal distribution of the emission rate were used in our simulations. The first release scenario was published in (Brandt et al., 2002), the second one in (Talerko, 2005), and the last one was recently proposed in (Evangelou et al., 2017). The former two parameterizations represent the CNPP releases by means of several point sources at different heights above the ground. In the (Brandt et al., 2002) source model there are 6 emission points at the altitudes of 225, 425, 715, 1090, 1575 and 2225 m above the ground level, whereas only 4 points, at 200, 500, 800 and 1200 m, are used in (Talerko, 2005). These parameterizations also differ in the time discretization. In the first source model, the emissions are specified on the daily scale, while Talerko defines emissions for every 6 h. Both schemes treat the ^{137}Cs release as a single particle fraction with mean diameter of $1\ \mu\text{m}$ and particle density of $2.5 \cdot 10^3\ \text{kg m}^{-3}$. Such particle parameters suggest that in order to simulate their dry removal, the constant deposition velocity of $0.005\ \text{m/s}$ can be assumed and used in simulations (Talerko, 2005). This value of the deposition velocity of the Chernobyl radioactive Cesium is consistent with the results previously reported in other publications (e.g. Izrael et al., 1990).

The (Evangelou et al., 2017) source parameterization is more sophisticated. Instead of point sources, 6 continuous vertical linear sources with length of 500 m were defined between 0 and 3000 m above the ground. Such representation of the Chernobyl emissions should be more accurate and consistent with the actual emissions. The source evolution time step is finer (3 h) than the previously published source models. Moreover, four fractions of radioactive ^{137}Cs aerosol particles with mean diameters of 0.4, 1.2, 1.8 and $5.0\ \mu\text{m}$ were defined and emission rates were provided for every fraction separately. The particle density of $2.5 \cdot 10^3\ \text{kg m}^{-3}$ was assumed for every fraction.

The emission rates on a daily temporal scale for every source scheme are presented in Fig. 2(a–c), where (Evangelou et al., 2017) the source emission rates were integrated over all size fractions. As can be seen from Fig. 2 (d) the adopted source parameterizations yield quite similar temporal behavior of the total daily emissions (integrated over the vertical coordinate). The vertical structure of the emission rates, however, differs significantly from one parametrization to another.

2.4. Evaluation data and model's performance statistical indices

Similarly to (Gaiotti et al., 2018), to assess the quality of the calculated results we used a set of cumulative deposition data measured at 410 sample sites on the territory of Ukraine (Fig. 3). The data were extracted from the complete dataset of ^{137}Cs contamination measurements conducted in the early 1990s using a combination of a soil sampling method and airborne gamma spectrometry (De Cort et al., 1998). As it can be seen from Fig. 3 the chosen set of verification points can replicate the geographical structure of the ^{137}Cs deposition pattern on the territory of Ukraine fairly well. All major radioactive traces

(Western, Eastern and Southern) and all significant local maxima of the contaminations are captured. This indicates that the evaluation dataset can be used for meaningful assessment of the simulation results.

Due to a vast range of deposition values (several orders of magnitude) it is preferable to use a complementary set of statistical indexes in order to obtain a reliable measure of a model's performance (Mosca et al., 1998). The following statistical tests and indices were employed in the present work: BIAS, geometric mean bias (MG), normalized mean square error (NMSE), geometric mean variance (VG), Pearson's correlation coefficient (PCC), PCC for data in log-scale (PCC_{lg}), factor of exceedance (FOEX), factor of 2 (FA2) and factor of 5 (FA5). Their detailed description can be found in (Mosca et al., 1998; Chang et al., 2003). All the tests were performed using pairs (M_i , C_i), $i = 1, \dots, 410$, where M_i and C_i are the measured and calculated ^{137}Cs total deposition at the i -th evaluation point respectively.

In addition to the indices we also evaluated the accuracy of the HYSPLIT-simulated geographic patterns of depositions using Figures of Merit in Space (FMS) (Mosca et al., 1998). FMSs were calculated for every contamination interval, according to the map legend in (De Cort et al., 1998), along with their generalized/weighted estimate, FMS_g (Gaiotti et al., 2018).

Lastly, the scatter diagrams, where calculated depositions are depicted against respective measured values, were also built to visually inspect the quality of the simulations results.

3. Simulation results

3.1. Sensitivity tests

In the first step of our study we performed a number of simulations (sensitivity tests), which included all combinations of the input meteorology, the source models and two approaches for dry deposition calculation (Table 1). In tests 1–9 the constant deposition velocity of $0.005\ \text{m/s}$ was used to simulate dry removal processes, whereas the resistance method was applied in tests 10–18.

The purpose of the sensitivity simulations was to tune the model and generate the best possible computational results (in terms of the final deposition pattern) for further analysis. We also wanted to determine how differences in the final deposition pattern depend on the input meteorology and source model used.

The values of the statistical indices for every simulation are provided in Tables 2 and 3. The values highlighted with bold font in these tables indicate the sensitivity tests with the best performance for each metric. As can be seen from the tables, the best performance was observed in test 2 (ERA meteorology/(Talerko, 2005) source/const. v_d). Five out of ten measures, namely VG, PCC_{lg} , FA2, FA5 and FMS_g (only the generalized estimate of FMS was taken into account) for this simulation reached their highest values. Even though the simulation yielded rather large negative BIAS ($-24.201\ \text{kBq m}^{-2}$, which we attribute to slightly underestimated values in the highest part of the deposition range) other statistics were relatively close to their best values. For instance, Pearson's correlation coefficient reached 0.849 and was almost 0.7 for the data in log-scale. FA5 was equal to 86%, which indicates that the majority of calculated deposition values do not differ from the measured ones by more than a factor of 5. The final accumulated deposition pattern for this simulation showed the largest consistency with the geographical distribution of the measured contaminations ($\text{FMS}_g = 22\%$).

Two more simulations, test 1 (WRF/(Talerko, 2005)/const. v_d) and test 8 (ERA/(Evangelou et al., 2017)/const. v_d), also showed rather good values of statistical indices. However, the total deposition structures generated in these simulations have larger spatial discrepancies with the measured contamination patterns (FMS_g equaled to 17% and 16% for test 1 and test 8 respectively).

The scatter diagrams and final deposition patterns for tests 1, 2, and 8 are shown in Figs. 4 and 5 respectively. It can be clearly seen from

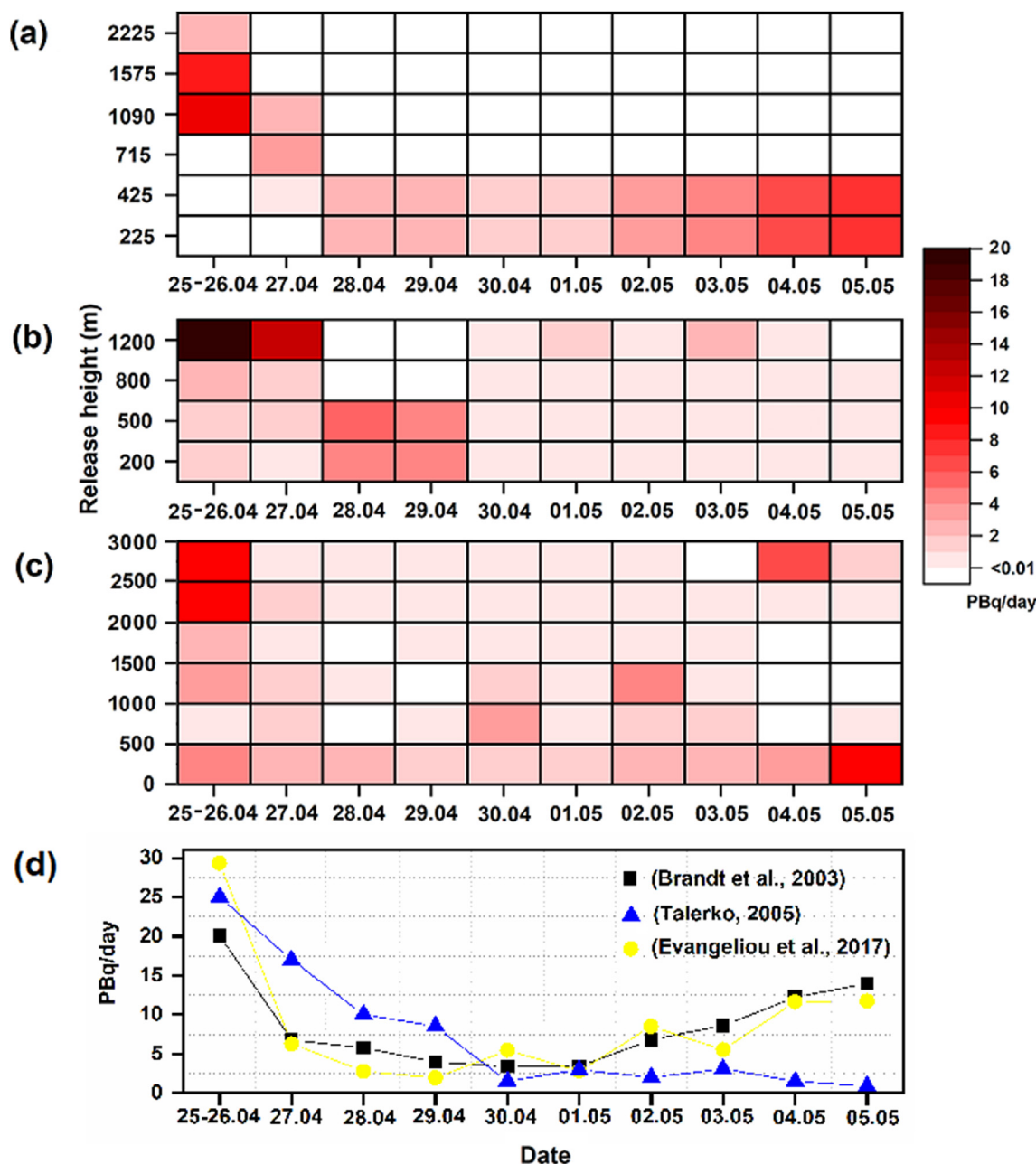


Fig. 2. Temporal and vertical distribution of the ¹³⁷Cs daily release rates during the CNPP accident: (a) (Brandt et al., 2002); (b) (Talerko, 2005); (c) (Evangeliou et al., 2017). The daily release rates integrated over the vertical coordinate (d). Note: the CNPP accident occurred on April 25 at 21:23 (UTC).

these figures that test 2 yielded the best performance.

The conclusions drawn from the results shown in Tables 2–3 and Figs. 4 and 5 can be summarized as follows:

We found an underestimation of depositions obtained with dry removal calculated based on the resistance method compared to the results obtained with the constant deposition velocity of 0.005 m/s and real measurements. Such conclusion is valid for all the tests except those, which use the WRF ARW meteorology. Both dry removal approaches in a combination with the output of the prognostic model give similar results. A possible reason for this might be the more precise and detailed information about the boundary layer structure calculated in the WRF ARW simulation compared to the reanalysis data. However, we would like to note that a significant underestimation of dry deposition of the Chernobyl ¹³⁷Cs particles calculated with the full resistant model has also been reported in many other studies (e.g. Brandt et al., 2002; Giaiotti et al., 2018). It would be interesting to consider

this issue in detail in a separate study.

The spatial resolution of the meteorological data has a very significant effect on the calculated deposition pattern. The simulation with NCAR/NCEP coarse gridded data (2.5°, ~250 km) yielded worse statistical indices compared to ERA Interim (0.75°, ~75 km) or WRF ARW (30 km) simulations. This is an expected result, because a big part of the depositions were created by means of atmospheric precipitations, whose spatial representation in the NCAR/NCEP reanalysis data is not dense enough. However, the differences between the simulations with the ERA and WRF input meteorology are not very noticeable. Moreover, the ERA data gives a more consistent geographical picture of the accumulated depositions compared to the WRF data (see Fig. 5 (b) and (c) respectively). The values of FMS_g are higher for the simulations with the ERA reanalysis data compared to the simulations with the WRF output for all three source models.

(Talerko, 2005) source model appears to be the most accurate one,

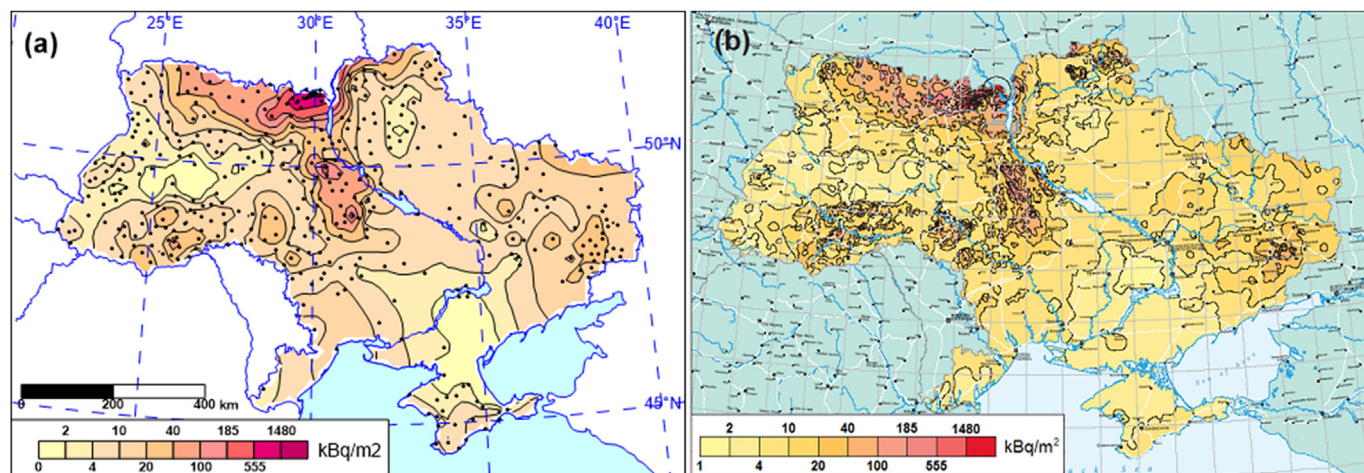


Fig. 3. (a) Location of 410 evaluation points (black dots) on the territory of Ukraine and the ¹³⁷Cs contamination pattern built on their base; (b) the ¹³⁷Cs contamination of Ukraine adapted from (De Cort et al., 1998) (from Gaiotti et al., 2018).

Table 1
Specifications of the sensitivity simulations.

N test	Meteorology	Source	Dry deposition calculation
1	WRF ARW	Talerko (2005)	const. v _d (0.005 m/s)
2	ERA Interim	Talerko (2005)	const. v _d (0.005 m/s)
3	NCAR NCEP	Talerko (2005)	const. v _d (0.005 m/s)
4	WRF ARW	Brandt et al. (2002)	const. v _d (0.005 m/s)
5	ERA Interim	Brandt et al. (2002)	const. v _d (0.005 m/s)
6	NCAR NCEP	Brandt et al. (2002)	const. v _d (0.005 m/s)
7	WRF ARW	Evangeliou et al. (2017)	const. v _d (0.005 m/s)
8	ERA Interim	Evangeliou et al. (2017)	const. v _d (0.005 m/s)
9	NCAR NCEP	Evangeliou et al. (2017)	const. v _d (0.005 m/s)
10	WRF ARW	Talerko (2005)	resist. method
11	ERA Interim	Talerko (2005)	resist. method
12	NCAR NCEP	Talerko (2005)	resist. method
13	WRF ARW	Brandt et al. (2002)	resist. method
14	ERA Interim	Brandt et al. (2002)	resist. method
15	NCAR NCEP	Brandt et al. (2002)	resist. method
16	WRF ARW	Evangeliou et al. (2017)	resist. method
17	ERA Interim	Evangeliou et al. (2017)	resist. method
18	NCAR NCEP	Evangeliou et al. (2017)	resist. method

at least for regional simulations on the spatial scale of ~1000 km from the source. Two of the three simulations that yielded the lowest

Table 2
Statistical tests of the global verification analysis.

N of test	BIAS	MG	NMSE	VG	PCC	PCC _{lg}	FOEX	FA2	FA5
	kBq/m ²	-	-	-	-	-	%	%	%
	Best 0	Best 1	Best 0	Best 1	Best 1	Best 1	Best 0	Best 100	Best 100
1	22.113	1.039	4.696	5.794	0.826	0.656	1	47	79
2	-24.201	0.928	6.518	3.694	0.849	0.692	-5	47	86
3	14.278	0.672	6.902	12.355	0.853	0.559	-7	39	70
4	-4.697	1.166	5.135	9.798	0.811	0.541	5	36	70
5	-32.001	0.985	12.343	7.407	0.785	0.545	2	35	75
6	19.605	1.156	6.051	69.867	0.735	0.333	8	26	55
7	-21.032	0.819	6.686	7.576	0.819	0.571	-2	37	72
8	-23.816	0.918	7.519	4.111	0.800	0.648	-1	42	85
9	4.866	1.095	4.324	10.598	0.829	0.542	4	34	72
10	10.212	1.029	4.687	5.835	0.802	0.651	1	42	78
11	-43.302	0.421	18.588	24.013	0.821	0.512	-21	27	63
12	-3.116	0.289	6.007	424.338	0.828	0.465	-20	27	51
13	25.421	1.346	6.079	17.804	0.765	0.517	6	30	59
14	-46.044	0.490	26.513	26.525	0.735	0.446	-16	27	61
15	-24.757	0.324	7.531	60.608	0.805	0.509	-26	24	56
16	-7.409	1.186	5.504	10.754	0.800	0.525	6	32	66
17	-49.856	0.607	32.716	15.850	0.802	0.423	-13	35	70
18	-29.938	0.336	8.456	34.118	0.825	0.594	-26	30	60

discrepancy with the measurements used this source parameterization. However, it should be noted that (Talerko, 2005) source model was designed specifically to reproduce the contamination pattern on the territory of Ukraine. Whether it is applicable at larger spatial scales (the entire European continent) remains to be seen. The third and most sophisticated source parameterization (Evangeliou et al., 2017) did not give any noticeable improvement of the predicted deposition pattern on the territory of Ukraine.

3.2. Relative contribution of wet and dry deposition processes to the contamination pattern formation on the territory of Ukraine

In our analysis of the removal processes at the stage of ¹³⁷Cs contamination formation on the territory of Ukraine we used only the simulations that gave the best statistical indices. Higher values of statistical indices (including FMS_g, the measure of spatial agreement between the predicted and measured deposition patterns) give more confidence in the predictive power of the simulation of the dispersion and deposition processes during active phase of the Chernobyl catastrophe. However, even in this case the results should be interpreted with caution because not all significant local maxima of the cumulative deposition pattern were reproduced. Some uncertainties remains present in the simulation results.

Table 3
Figure of merit in space (FMS, %) for simulations.

N of test	Limiting significant levels of total deposition, kBq/m ²										FMS _g Best 100
	0–2	2–4	4–10	10–20	20–40	40–100	100–185	185–555	555–1480	> 1485	
1	6	16	27	14	6	17	0	7	30	25	17
2	16	29	24	21	14	14	9	0	35	50	22
3	12	17	25	7	5	8	6	0	43	33	16
4	3	23	22	5	8	5	0	0	56	0	15
5	23	26	14	18	6	6	4	0	33	0	17
6	12	17	15	8	4	6	9	2	0	25	12
7	13	18	16	12	7	19	11	0	12	50	15
8	20	19	16	17	8	3	0	0	12	50	16
9	14	3	20	17	4	5	0	0	47	100	13
10	5	18	24	11	10	14	0	9	42	50	16
11	7	14	9	14	3	7	4	0	0	0	10
12	13	8	23	4	8	25	4	0	40	100	14
13	12	22	14	8	8	8	7	0	42	50	13
14	9	13	6	27	7	8	0	0	0	0	12
15	14	6	14	9	1	6	0	0	30	100	10
16	4	16	16	14	6	12	10	0	35	50	13
17	7	14	13	14	7	5	0	0	0	0	12
18	12	6	20	15	10	4	0	0	18	50	13

As can be seen from Fig. 5 (b) the HYSPLIT three-dimensional particle model coupled with the ERA-Interim reanalysis meteorological data (Talerko, 2005), source model and constant deposition velocity of 0.005 m/s was capable of reproducing the main radioactive traces (Western, Eastern and Southern, listed in a chronological order of their occurrence) on the territory of Ukraine with good accuracy. Several secondary (those that are far away from the source) local maxima were also reproduced. For instance, the local maxima in the Eastern part of Ukraine and in the Ukrainian Carpathians are clearly visible. However, the significant secondary local maximum in the Southern trace does not appear clearly.

In order to determine the physical mechanisms (dry or wet, both in-cloud and below-cloud) responsible for the appearance of the radioactive traces and local maxima, we conducted two additional simulations. They were similar to test 2 but had dry deposition set to zero. In the first simulation (the corresponding cumulative deposition pattern is shown in Fig. 6 (a)) both wet removal (in/below-cloud) processes were taken into account, whereas in the second simulation (Fig. 6 (c)) only the in-cloud wet removal scheme was applied. Moreover, in each of these additional simulations we also computed the ratio between the calculated deposition values and the total depositions obtained in test 2 (with dry and wet removal processes taken into account). The calculated results are shown in Fig. 6 (b, d). The scatter diagrams for these additional simulations are presented in Fig. 7.

Fig. 6 (b, d) shows that the ratio between wet and total depositions is larger than unity on the significant part of the domain. It is not an artefact of the simulations. It is a consequence of formula (1) being applied in HYSPLIT to calculate wet and dry removal of pollutants. The formula is not additive with respect to different removal processes, which means that wet and dry depositions can be calculated separately in HYSPLIT, but their sum can differ from the total depositions (HYSPLIT, 2018). When simulating dispersion of aerosol particles with dry deposition set to zero, more pollutants will remain in the atmosphere compared to the case when dry removal is taken into account. Therefore, the same amount of precipitation can deposit a larger amount of pollutant, in particular far away from the source. Thus, the results presented in Fig. 6 should only be looked at in relative terms (i.e. just to see what kind of removal processes played a more significant role) and not as an accurate map of absolute deposition values.

According to Fig. 6, wet removal processes contributed to the formation of the western trace on the territory of Ukraine. However, dry depositions played a significant role here as well. It can be explained if we assume that this trace was created in the first day of the catastrophe when the relatively large radioactive debris (with large settling/deposition velocity) occurred after the explosion, transported and deposited along the mean wind direction.

The Eastern trace was created mainly due to wet removal processes. Wet/total deposition ratio is larger than unity almost everywhere in the

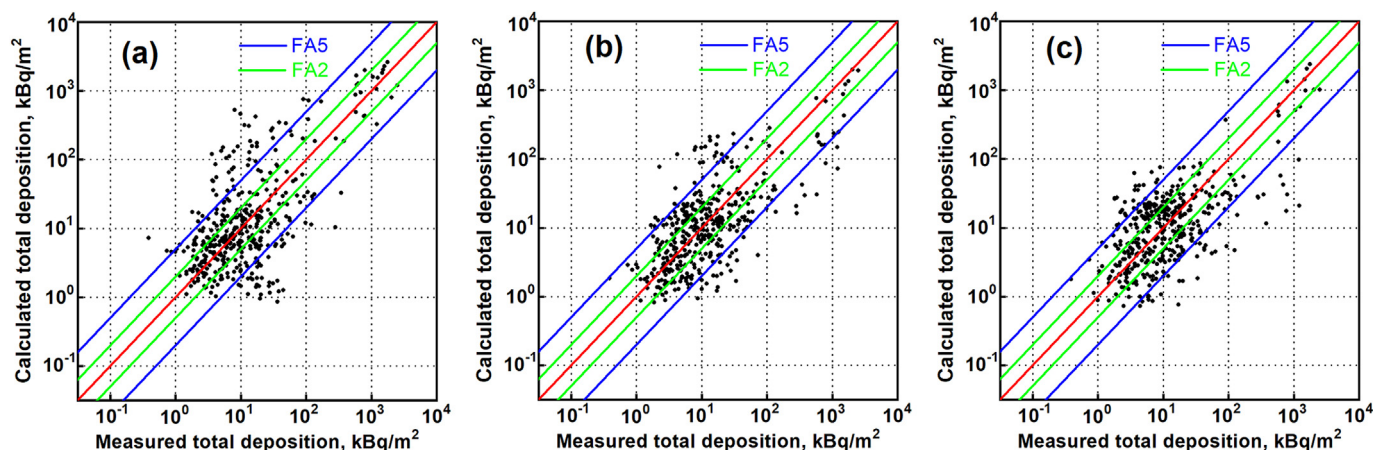


Fig. 4. Scatter diagrams for selected simulations: (a) test 1 (WRF/(Talerko, 2005)/const.v_d), (b) test 2 (ERA/(Talerko, 2005)/const.v_d); (c) test 8 (ERA/(Evangeliou et al., 2017)/const.v_d).

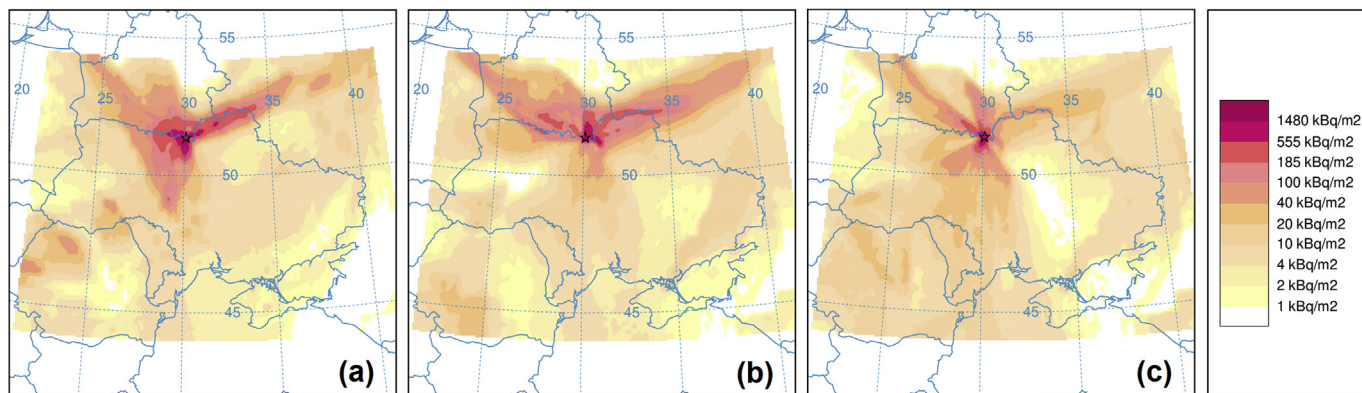


Fig. 5. Cumulative (integrated from 2100 25 April to 2300 6 May 86 UTC) ¹³⁷Cs deposition pattern for selected HYSPLIT simulations: (a) test 1 (WRF/(Talerko, 2005)/const.v_d), (b) test 2 (ERA/(Talerko, 2005)/const.v_d); (c) test 8 (ERA/(Evangeliou et al., 2017)/const.v_d). A star marks the source location.

Eastern part of the domain including Eastern Ukraine. Wet deposition is also a key mechanism for the appearance of a local maximum in the Ukrainian Carpathians.

The southern trace on the territory of Ukraine is primarily caused by dry depositions. It is likely that dry depositions were also responsible for a significant secondary local maximum in this trace. However, because this local maximum was not visible very clearly in our simulations it is hard to make a definite conclusion regarding its nature. Some ideas aiming to explain the existence of this local maximum have been proposed previously (e.g. Buikov et al., 1992; Voloshchuk and Shkvorets, 1993; Skrynyk et al., 2010). Nevertheless, the mechanism of its creation still remains unclear and needs to be considered in a separate study.

In general, we may conclude that dry deposition played an

important role in the contamination formation on the territory of Ukraine. It is confirmed by the scatter diagrams presented in Fig. 7. To quantify in an approximate way the contribution of wet total (in-cloud + below-cloud) and wet in-cloud removals to the total contamination we calculated an amount of ¹³⁷Cs deposited on the surface based on gridded values of cumulative depositions shown in Fig. 5 (b), 6 (a) and 6 (c). We performed the calculations separately for the whole modeling domain and the territory of Ukraine only. According to our estimates, the wet total (in-cloud + below-cloud) removal accounts for ~61% of the contamination on the domain (~46% on the territory of Ukraine), while wet in-cloud removal can explain ~47% of ¹³⁷Cs deposited on the domain (~25% on the territory of Ukraine). We would like to note it again that these numbers should be interpreted as a rough estimate (probably, as an upper limit) because of nonadditivity of

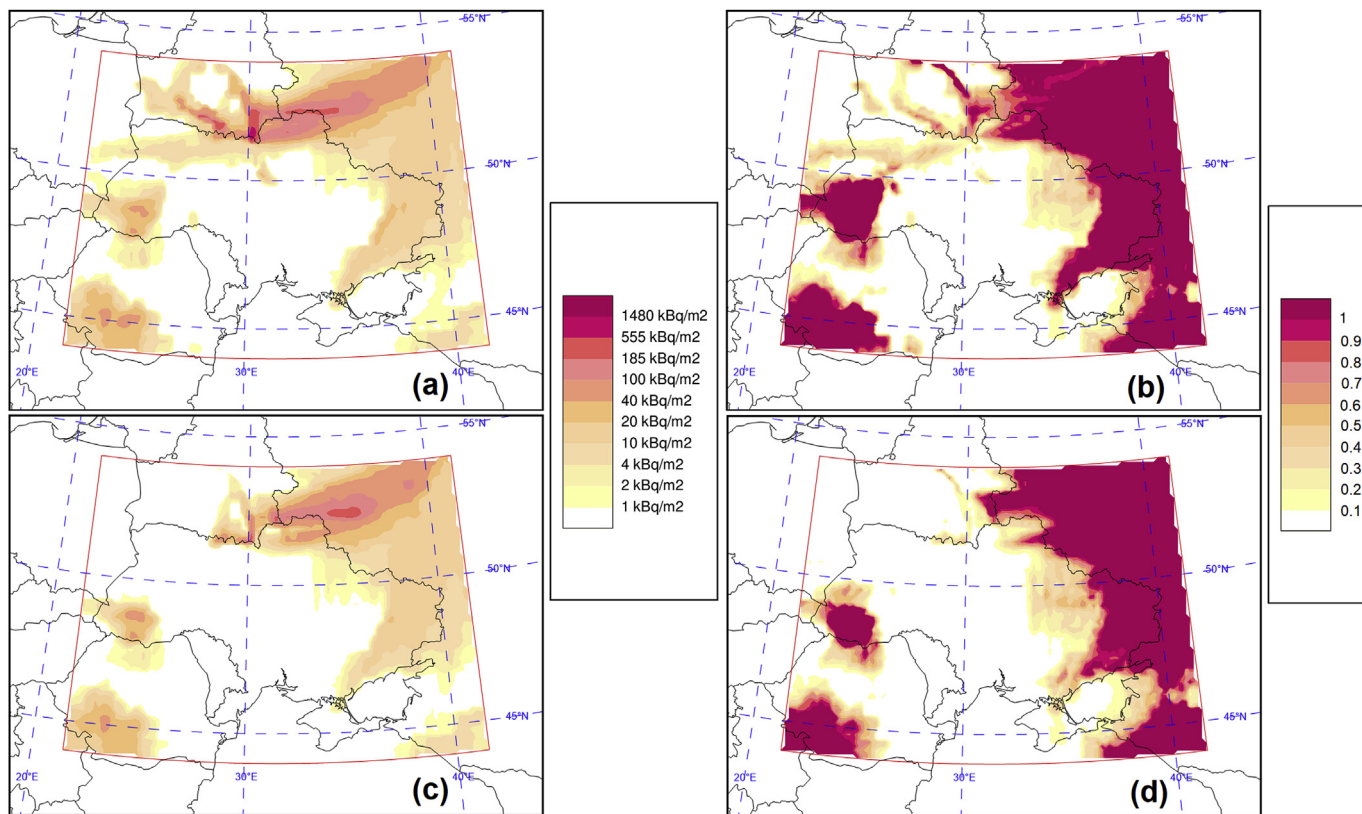


Fig. 6. (a) Cumulative (integrated from 2100 25 April to 2300 6 May 86 UTC) ¹³⁷Cs wet deposition pattern resulted from the simulation similar to test 2 (ERA/(Talerko, 2005)/const.v_d) but with dry depositions set to zero; (b) ratio between the cumulative wet and total depositions on the domain; (c) same as (a) but when wet in-cloud removal was simulated; (d) same as (b) but only when wet in-cloud removal was simulated.

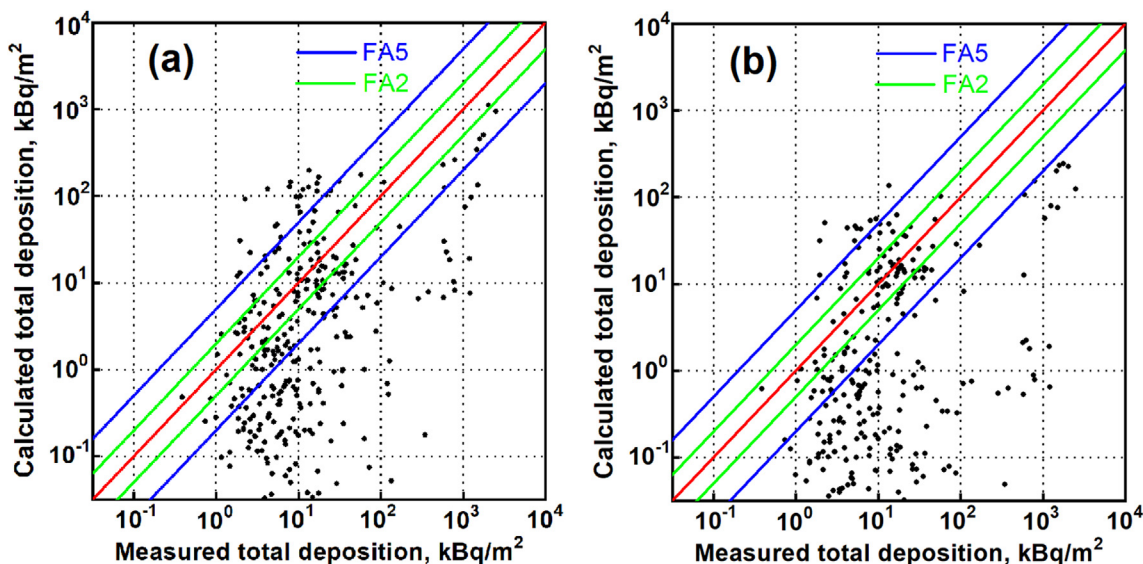


Fig. 7. Scatter diagram for simulations when only wet total (in-cloud + below-cloud) (a) and wet in-cloud removal were taken into account.

formula (1) regarding removal processes. However, the estimate shows that dry depositions constitute a significant part of cumulative depositions (approximately one half of the total depositions on the territory of Ukraine). Such the estimate is significantly larger than those reported in previous works (e.g. Draxler and Hess, 1998; Lauritzen and Mikkelsen, 1999), where a substantial overbalance of wet removal processes compared to dry ones during the deposition of the Chernobyl ^{137}Cs was reported. For instance, according to the assessment conducted in (Lauritzen and Mikkelsen, 1999) $\sim 90\%$ of the total depositions of ^{137}Cs on the European scale after the CNPP accident stems from wet deposition and only $\sim 10\%$ was due to dry deposition, whereas in (Draxler and Hess, 1998) the ratio between dry and wet removal was 1/3.

It should be mentioned that our conclusion about the significance of dry deposition is not totally surprising and does not necessarily contradict to the above-mentioned studies. Our assessment concerns the regional scale dispersion processes (~ 1000 km from the source), where dry deposition is known to be an important factor, whereas the estimates (Draxler and Hess, 1998; Lauritzen and Mikkelsen, 1999) were made based on simulations where the source is far away. In general it can be assumed that the larger the distance from the source, the less is the contribution of dry depositions. One of the reasons for such conclusion might be the vertical dispersion which decreases near-surface air pollutant concentration and thus dry deposition amount in downwind regions.

It is also interesting to note that according to our results, both in-cloud and below-cloud wet removals had approximately equal contribution to the radioactivity deposition on the territory of Ukraine (but in-cloud removal is slightly more important on the whole domain). This means that pollutants were well mixed across the lowest part of the atmosphere (they were not concentrated only in the PBL or just above the PBL). On the other hand, such results may also point out the importance of the convective precipitations (rain-out scavenging processes) in the removal processes.

3.3. Qualitative comparison with CALPUFF results

A simulation of the Chernobyl ^{137}Cs dispersion and deposition processes over the territory of Ukraine was recently reported by Gaiotti (Gaiotti et al., 2018). That simulation employed the CALPUFF model. CALPUFF is a dispersion modeling system that is based completely on puff representation of the pollutant releases. According to (Gaiotti et al., 2018) the model was able to capture the main radioactive traces on the territory of Ukraine. The final deposition pattern appeared to be

oversmoothed, however. It was speculated that the oversmoothing could come from the calculating algorithm for wet depositions applied in CALPUFF. Therefore, it would be interesting to compare the CALPUFF results with some other Lagrangian dispersion model such as HYSPLIT, that can be applied in the same computational mode (the pure puff approach).

In Fig. 8 (a) and (b) the final ^{137}Cs deposition patterns calculated with HYSPLIT (puff mode in both vertical and horizontal directions) and CALPUFF are presented respectively. In these simulations the same ^{137}Cs release scenario, namely (Talerko, 2005), and gridded meteorology, namely the WRF ARW outputs, were used for both models. We should emphasize that the WRF ARW data was the only possible option to apply the same meteorology to both dispersion models. This is because CALPUFF cannot accept reanalysis data. HYSPLIT can be fed with WRF ARW calculated results directly, whereas CALPUFF adopts such meteorology through the meteorological preprocessor CALMET. To prevent CALMET from distorting the gridded meteorological field we used recommendations published in (Scire et al., 2012). In addition, both models were tuned to simulate dry removal of pollutants through the constant deposition velocity of 0.005 m/s and wet removal through the scavenging coefficient of $8 \cdot 10^{-5} \text{ s}^{-1}$. The CALPUFF simulation was performed with the puff split option activated, whereas HYSPLIT applies puff splitting by default.

As can be seen in Fig. 8, even when using the pure puff mode, the HYSPLIT cumulative deposition pattern appears to be more consistent with the actual contamination pattern than that of CALPUFF. Radioactive traces and local maxima in the HYSPLIT-predicted cumulative depositions are clearly seen whereas the CALPUFF-generated deposition pattern is clearly oversmoothed.

We should note that we did not make any quantitative comparison of HYSPLIT and CALPUFF results based on the measured deposition data. According to our results, the combination of the WRF ARW meteorology and (Talerko, 2005) source model was not the one that produced the best contamination pattern. Hence, it was of little practical value to compare these calculated results with measurements. Such a comparison would not give us any new information about the deposition processes. The main focus of this section was just to make a relative comparison at the qualitative level and show that the CALPUFF computational algorithm for wet depositions must be modified (as it was pointed in (Gaiotti et al., 2018)) if the fine details of the spatial structure of the depositions far away from the source need to be reproduced.

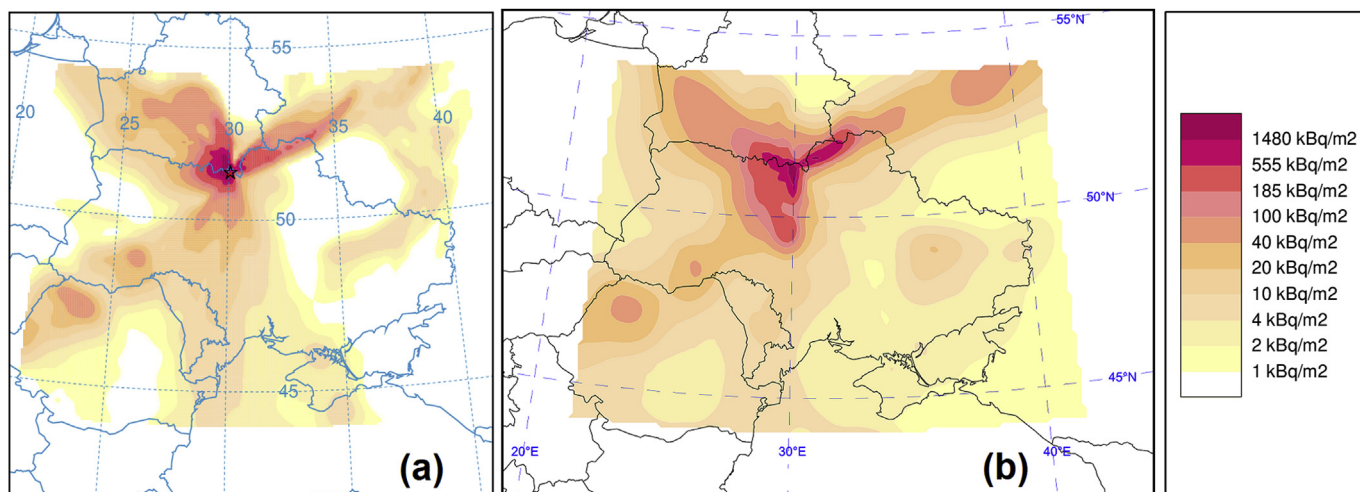


Fig. 8. HYSPLIT (full puff mode) (a) and CALPUFF (b) final deposition patterns.

4. Conclusion

This work reports simulations of the Chernobyl ^{137}Cs transport, dispersion, and deposition on the regional scale (the territory of Ukraine) performed with HYSPLIT model. Three datasets of gridded meteorology and three scenarios of pollutant releases published previously in the literature were used as input information for the simulations. The main focus of our study was the deposition patterns and associated physical mechanism. To simulate dry removal of radioactive aerosol particles we used a constant deposition velocity of 0.005 m/s and applied an approach based on the resistance method. The wet removal (both in-cloud and below-cloud) was modeled based on the same approach using the scavenging constant of $8 \cdot 10^{-5} \text{ s}^{-1}$.

The results of our simulations show that both the meteorology and pollutant source parameterization have a very significant influence on the ^{137}Cs accumulated deposition pattern that comes out of HYSPLIT. According to the statistical evaluation and visual inspection of our predicted contamination patterns the result that agreed best with the measurements was obtained with the ERA-Interim reanalysis data (Talerko, 2005), source model and a constant deposition velocity of 0.005 m/s. In this simulation the main radioactive traces and nearly all significant secondary local maxima on the territory of Ukraine were reproduced. Similar values of the statistical indices were also obtained in the simulations where the combinations WRF/(Talerko, 2005)/const. v_d and ERA/(Evangelio et al., 2017)/const. v_d of input information were used. However, the total deposition structures generated in the latter simulations have larger spatial discrepancies with the measured contamination pattern. It should be noted that the use of high-resolution meteorological data (WRF simulation) and more detailed information regarding pollutant emissions did not improve HYSPLIT predictions.

We have found that the application of the constant deposition velocity of 0.005 m/s gives much better consistency of the calculated contamination pattern compared to when an approach based on the resistance method is used. In the latter case an underestimation of the calculated depositions occurs.

Our simulations also showed that dry deposition played a significant role during the contamination formation on the territory of Ukraine. According to our estimates, approximately 50% of the total depositions are due to dry removal processes. The relative influence of wet in-cloud and below-cloud removal was about the same.

These new HYSPLIT simulations have improved our understanding of the physical mechanisms and conditions of the ^{137}Cs contamination formation in Ukraine after the Chernobyl catastrophe. However, the elucidation of how some local maxima in the Southern radioactive trace

were formed remains a difficult task. We believe that further simulations may help shed light on these unresolved issues and clarify the mechanisms of the radioactivity removal on the regional scale after the Chernobyl accident.

Lastly, we can report that the overall performance of the HYSPLIT model in terms of the deposition calculations was rather good. We believe it can be used successfully in other deposition studies on the regional scales.

Acknowledgements

This work has been partially supported by the Ministry of Education and Science of Kazakhstan (state-targeted program BR05236454 “Center of Excellence for Fundamental and Applied Physics”) and Nazarbayev University faculty development grant (090118FD5345). The authors are grateful to anonymous reviewers for careful reading of the manuscript and valuable comments and suggestions they have made.

References

- Arnold, D., Maurer, C., Wotawa, G., Draxler, R., Saito, K., Seibert, P., 2015. Influence of the meteorological input on the atmospheric transport modelling with FLEXPART of radionuclides from the Fukushima Daiichi nuclear accident. *J. Environ. Radioact.* 139, 212–225. <https://doi.org/10.1016/j.jenvrad.2014.02.013>.
- Baklanov, A., Sørensen, J.H., 2001. Parameterization of radionuclide deposition in atmospheric long-range transport modeling. *Phys. Chem. Earth B* 26 (10), 787–799. [https://doi.org/10.1016/S1464-1909\(01\)00087-9](https://doi.org/10.1016/S1464-1909(01)00087-9).
- Brandt, J., Christensen, J.H., Frohn, L.M., 2002. Modeling transport and deposition of caesium and iodine from the Chernobyl accident using the DREAM model. *Atmos. Chem. Phys.* 2, 397–417. <https://doi.org/10.5194/acp-2-397-2002>.
- Buikov, M.V., Garger, E.K., Talerko, N.N., 1992. Research into the formation of spotted pattern of radioactive fallout with the Lagrangian-Eulerian model. *Russ. Meteorol. Hydrol.* 12, 33–45.
- Chen, F., Dudhia, J., 2001. Coupling and advanced land surface-hydrology model with the Penn State-NCAR MM5 modeling system. Part I: model implementation and sensitivity. *Mon. Weather Rev.* 129, 569–585. [https://doi.org/10.1175/1520-0493\(2001\)129<0569:CAALSH>2.0.CO;2](https://doi.org/10.1175/1520-0493(2001)129<0569:CAALSH>2.0.CO;2).
- Chang, J., Franzese, P., Chayantrakom, K., Hanna, S., 2003. Evaluations of CALPUFF, HPAC, and VLSTRACK with two mesoscale field datasets. *J. Appl. Met.* 42, 453–466. [https://doi.org/10.1175/1520-0450\(2003\)042<0453:EOCHAV>2.0.CO;2](https://doi.org/10.1175/1520-0450(2003)042<0453:EOCHAV>2.0.CO;2).
- De Cort, et al., 1998. *The Atlas of Caesium-137 Contamination of Europe after the Chernobyl Accident*. Office for Official Publication of the European Communities, Luxembourg.
- Dee, D.P., Uppala, S.M., Simmons, A.J., Berrisford, P., Poli, P., Kobayashi, S., Andrae, U., Balmaseda, M.A., Balsamo, G., Bauer, P., Bechtold, P., Beljaars, A.C.M., van de Berg, L., Bidlot, J., Bormann, N., Delsol, C., Dragani, R., Fuentes, M., Geer, A.J., Haimberger, L., Healy, S.B., Hersbach, H., Hólm, E.V., Isaksen, I., Kållberg, P., Köhler, M., Matricardi, M., McNally, A.P., Monge-Sanz, B.M., Morcrette, J.-J., Park, B.-K., Peubey, C., de Rosnay, P., Tavolato, C., Thépaut, J.-N., Vitart, F., 2011. The ERA-Interim reanalysis: configuration and performance of the data assimilation system. *Q. J. R. Meteorol. Soc.* 137, 553–597. <https://doi.org/10.1002/qj.828>.

- Draxler, R.R., Hess, G.D., 1998. An overview of the Hysplit 4 modeling system for trajectories, dispersions, and deposition. *Aust. Meteorol. Mag.* 47, 295–308.
- Draxler, R.R., 1999. HYSPLIT4 User's Guide. NOAA Tech. Memo. ERL ARL-230. NOAA Air Resources Laboratory, Silver Spring, MD.
- Draxler, R.R., Rolph, G.D., 2012. Evaluation of the Transfer Coefficient Matrix (TCM) approach to model the atmospheric radionuclide air concentrations from Fukushima. *J. Geophys. Res.* 117, D05107. <https://doi.org/10.1029/2011JD017205>.
- Draxler, R.R., Arnold, D., Chino, M., Galmarini, S., Hort, M., Jones, A., Leadbetter, S., Malo, A., Maurer, C., Rolph, G., Saito, K., Servranckx, R., Shimbori, T., Solazzo, E., Wotawa, G., 2013. World Meteorological Organization's model simulations of the radionuclide dispersion and deposition from the Fukushima Daiichi nuclear power plant accident. *J. Environ. Radioact.* 139, 172–184. <https://doi.org/10.1016/j.jenvrad.2013.09.014>.
- Draxler, R.R., Hess, G.D., 2017. Description of the HYSPLIT_4 Modeling System. NOAA Tech. Memo. ERL ARL-224. NOAA Air Resources Laboratory, Silver Spring, MD.
- Evangelou, N., Balkanski, Y., Cozic, A., Möller, A.P., 2013. Simulations of the transport and deposition of ¹³⁷Cs over Europe after the Chernobyl Nuclear Power Plant accident: influence of varying emission-altitude and model horizontal and vertical resolution. *Atmos. Chem. Phys.* 13, 7183–7198. <https://doi.org/10.5194/acp-13-7183-2013>.
- Evangelou, N., Hamburger, T., Talerko, N., Zibtsev, S., Bondar, Y., Stohl, A., Balkanski, Y., Mousseau, T.A., Möller, A.P., 2016. Reconstructing the Chernobyl Nuclear Power Plant (CNPP) accident 30 years after. A unique database of air concentration and deposition measurements over Europe. *Environ. Pollut.* 216, 408–418. <https://doi.org/10.1016/j.envpol.2016.05.030>.
- Evangelou, N., Hamburger, T., Cozic, A., Balkanski, Y., Stohl, A., 2017. Inverse modeling of the Chernobyl source term using atmospheric concentration and deposition measurements. *Atmos. Chem. Phys.* 17, 8805–8824. <https://doi.org/10.5194/acp-17-8805-2017>.
- Geng, X., Xie, Z., Zhang, L., 2017. Influence of emission rate on atmospheric dispersion modeling of the Fukushima Daiichi Nuclear Power Plant accident. *Atmos. Pollut. Res.* 8 (3), 439–445. <https://doi.org/10.1016/j.apr.2016.10.013>.
- Gaiotti, D., Oshurok, D., Skrynyk, O., 2018. The Chernobyl nuclear accident ¹³⁷Cs cumulative depositions simulated by means of the CALMET/CALPUFF modelling system. *Atmos. Pollut. Res.* 9 (3), 502–512. <https://doi.org/10.1016/j.apr.2017.11.007>.
- Grell, G.A., Freitas, S.R., 2014. A scale and aerosol aware stochastic convective parameterization for weather and air quality modeling. *Atmos. Chem. Phys.* 14, 5233–5250. <https://doi.org/10.5194/acp-14-5233-2014>.
- Hong, S.Y., Noh, Y., Dudhia, J., 2006. A new vertical diffusion package with an explicit treatment of entrainment processes. *Mon. Weather Rev.* 134, 2318–2341. <https://doi.org/10.1175/MWR3199.1>.
- HYSPLIT, 2018. HYSPLIT Video Tutorial. <https://www.ready.noaa.gov/documents/Videos/index.html> accessed in December 2018.
- Iacono, M.J., Delamere, J.S., Mlawer, E.J., Shephard, M.W., Clough, S.A., Collins, W.D., 2008. Radiative forcing by long-lived greenhouse gases: calculations with the AER radiative transfer models. *J. Geophys. Res.* 113, D13103. <https://doi.org/10.1029/2008JD009944>.
- Izrael, Y.A., Vakulovsky, S.M., Vetrov, V.A., Petrov, V.N., Rovinskii, F.Y., Stukin, E.D., 1990. Chernobyl: Radioactive Contamination of the Environment. Hydrometeoizdat, Leningrad, 5-286-00799-6pp. 296 (In Russian).
- JRC, 2019. Radioactivity environmental monitoring (REM) web site. European union – joint research center. Available at: <https://rem.jrc.ec.europa.eu/RemWeb/>.
- Kajino, M., Sekiyama, T.T., Mathieu, A., Korsakissok, I., Pérrillat, R., Quélo, D., Quérel, A., Saunier, O., Adachi, K., Girard, S., Maki, T., Yumimoto, K., Didier, D., Masson, O., Igarashi, Y., 2018. Lessons learned from atmospheric modeling studies after the Fukushima nuclear accident: ensemble simulations, data assimilation, elemental process modeling, and inverse modeling. *Geochem. J.* 52, 1–17. <https://doi.org/10.2343/geochemj.2.0503>.
- Kalnay, E., Kanamitsu, M., Kistler, R., Collins, W., Deaven, D., Gandin, L., Iredell, M., Saha, S., White, G., Woollen, J., Zhu, Y., Chelliah, M., Ebisuzaki, W., Higgins, W., Janowiak, J., Mo, K.C., Ropelewski, C., Wang, J., Leetmaa, A., Reynolds, R., Jenne, R., Joseph, D., 1996. The NCEP/NCAR 40-year reanalysis project. *Bull. Am. Meteorol. Soc.* 77, 437–471. [https://doi.org/10.1175/1520-0477\(1996\)077<0437:TNYRP>2.0.CO;2](https://doi.org/10.1175/1520-0477(1996)077<0437:TNYRP>2.0.CO;2).
- Katata, G., Chino, M., Kobayashi, T., Terada, H., Ota, M., Nagai, H., Kajino, M., Draxler, R., Hort, M.C., Malo, A., Torii, T., Sanada, Y., 2015. Detailed source term estimation of the atmospheric release for the Fukushima Daiichi Nuclear Power Station accident by coupling simulations of an atmospheric dispersion model with an improved deposition scheme and oceanic dispersion model. *Atmos. Chem. Phys.* 15, 1029–1070. <https://doi.org/10.5194/acp-15-1029-2015>.
- Kinoshita, N., Sueki, K., Sasa, K., Kitagawa, J., Ikarashi, S., Nishimura, T., Wong, Y.-S., Satou, Y., Handa, K., Takahashi, T., Sato, M., Yamagata, T., 2011. Assessment of individual radionuclide distributions from the Fukushima nuclear accident covering central-east Japan. *Proc. Natl. Acad. Sci. U.S.A.* 108, 19526–19529. <https://doi.org/10.1073/pnas.1111724108>.
- Kinsler, A.M., 2001. Simulating Wet Deposition of Radiocesium from the Chernobyl Accident. M.S. thesis, Graduate School of Engineering and Management, Air Force Institute of Technology, pp. 108. pp. [Available online at: www.dtic.mil/get-tr-doc/pdf?AD=ADA392534].
- Klug, W., Graziani, G., Grippa, G., Pierce, D., Tassone, C., 1992. Evaluation of Long-Range Atmospheric Transport Models Using Environmental Radioactivity Data from the Chernobyl Accident. The ATMES Report. Elsevier applied science, London and New York, 1-85166-766-0pp. 370.
- Kovalets, I., Robertson, L., Persson, C., Didkivska, S., Ievdin, I., Trybushnyi, D., 2014. Calculation of the far range atmospheric transport of radionuclides after the Fukushima accident with the atmospheric dispersion model MATCH of the JRODOS system. *Int. J. Environ. Pollut.* 54 (2/3/4), 101–109. <https://doi.org/10.1504/IJEP.2014.065110>.
- Lauritzen, B., Mikkelsen, T., 1999. A probabilistic dispersion model applied to the long-range transport of radionuclides from the Chernobyl accident. *Atmos. Environ.* 33, 3271–3279. [https://doi.org/10.1016/S1352-2310\(99\)00108-9](https://doi.org/10.1016/S1352-2310(99)00108-9).
- Leadbetter, S.L., Hort, M.C., Jones, A.R., Webster, H.N., Draxler, R.R., 2015. Sensitivity of the modelled deposition of Caesium-137 from the Fukushima Daiichi nuclear power plant to the wet deposition parameterisation in NAME. *J. Environ. Radioact.* 139, 200–211. <https://doi.org/10.1016/j.jenvrad.2014.03.018>.
- Leelőssy, A., Lagzi, I., Kovács, A., Mészáros, R., 2018. A review of numerical models to predict the atmospheric dispersion of radionuclides. *J. Environ. Radioact.* 182, 20–33. <https://doi.org/10.1016/j.jenvrad.2017.11.009>.
- Masson, O., Baeza, A., Bieringer, J., Brudecki, K., Bucci, S., Cappai, M., Carvalho, F.P., Connan, O., Cosma, C., Dalheimer, A., Didier, D., Depuydt, G., De Geer, L.E., De Vismes, A., Gini, L., Groppi, F., Gudnason, K., Gurriaran, R., Hainz, D., Halldórsson, Ó., Hammond, D., Hanley, O., Holeý, K., Homoki, Z., Ioannidou, A., Isajenko, K., Jankovic, M., Katzlberger, C., Kettunen, M., Kierepko, R., Kontro, R., Kwakman, P.J.M., Lecomte, M., Leon Vintro, L., Leppänen, A.-P., Lind, B., Lujaneni, G., Mc Ginnity, P., Mc Mahon, C., Malá, H., Manenti, S., Manolopoulou, M., Mattila, A., Mauring, A., Mietelski, J.W., Møller, B., Nielsen, S.P., Nikolic, J., Overwater, R.M.W., Pálsson, S.E., Papastefanou, C., Penev, I., Pham, M.K., Povinec, P.P., Ramebäck, H., Reis, M.C., Ringer, W., Rodriguez, A., Rulík, P., Saey, P.R.J., Samsonov, V., Schlosser, C., Sgorbati, G., Silobritiene, B.V., Söderström, C., Sogni, R., Solier, L., Sonck, M., Steinhäuser, G., Steinkopff, T., Steinmann, P., Stoulos, S., Sýkora, I., Todorovic, D., Tooloutalaie, N., Tositti, L., Tschiersch, J., Ugron, A., Vagena, E., Vargas, A., Wershofen, H., Zhukova, O., 2011. Tracking of airborne radionuclides from the damaged Fukushima Daiichi nuclear reactors by European networks. *Environ. Sci. Technol.* 45 (18), 7670–7677. <https://doi.org/10.1021/es2017158>.
- Moroz, B.E., Beck, H.L., Bouville, A., Simon, S.L., 2010. Predictions of dispersion and deposition of fallout from nuclear testing using the NOAA-HYSPLIT meteorological model. *Health Phys.* 99 (2), 252–269. <https://doi.org/10.1097/HP.0b013e3181b43697>.
- Mosca, S., Graziani, G., Klug, W., Bellasio, R., Bianconi, R., 1998. A statistical methodology for the evaluation of long-range dispersion models: an application to the ETEX exercise. *Atmos. Environ.* 32 (24), 4307–4324. [https://doi.org/10.1016/S1352-2310\(98\)00179-4](https://doi.org/10.1016/S1352-2310(98)00179-4).
- Pudykiewicz, J., 1988. Numerical simulation of the transport of radioactive cloud from the Chernobyl nuclear accident. *Tellus B* 40, 241–259.
- Rolph, G.D., Ngan, F., Draxler, R.R., 2014. Modeling the fallout from stabilized nuclear clouds using the HYSPLIT atmospheric dispersion model. *J. Environ. Radioact.* 136, 41–55. <https://doi.org/10.1016/j.jenvrad.2014.05.006>.
- Saha, S., Moorthi, S., Pan, H.-L., Wu, X., Wang, J., Nadiga, S., Tripp, P., Kistler, R., Woollen, J., Behringer, D., Liu, H., Stokes, D., Grumbine, R., Gayno, G., Wang, J., Hou, Y.-T., Chuang, H.-Y., Juang, H.-M., Sela, J., Iredell, M., Treadon, R., Kleist, D., Van Delst, P., Keyser, D., Derber, J., Ek, M., Meng, J., Wei, H., Yang, R., Lord, S., Dool, H., Kumar, A., Wang, W., Long, C., Chelliah, M., Xue, Y., Huang, B., Schemm, J.-K., Ebisuzaki, W., Lin, R., Xie, P., Chen, M., Zhou, S., Higgins, W., Zou, C.-Z., Liu, Q., Chen, Y., Han, Y., Cucurull, L., Reynolds, R.W., Rutledge, G., Goldberg, M., 2010. The NCEP climate forecast system reanalysis. *Bull. Am. Meteorol. Soc.* 91, 1015–1057. <https://doi.org/10.1175/2010BAMS3001.1>.
- Scire, J.S., Strimatis, D.G., Wu, Z.-X., Klausmann, A., Popovic, E., 2012. Assessment of EPA's ETEX evaluation study. In: 10th Conference of Air Quality Models. RTP, North Carolina March 14-16, 2012.
- Simsek, V., Pozzoli, L., Unal, A., Kindap, T., Karaca, M., 2014. Simulation of ¹³⁷Cs transport and deposition after the Chernobyl nuclear power plant accident and radiological doses over the anatolian peninsula. *Sci. Total Environ.* 499, 74–88. <https://doi.org/10.1016/j.scitotenv.2014.08.038>.
- Skamarock, W.C., Klemp, J.B., 2008. A time-split nonhydrostatic atmospheric model for weather research and forecasting applications. *J. Comput. Phys.* 227 (7), 3465–3485. <https://doi.org/10.1016/j.jcp.2007.01.037>.
- Skrynyk, O., Chernysh, R., Hrytsyuk, Y., 2010. Formation of a large scale spot-like structure of the total deposition due to a powerful elevated finite source. *Adv. Sci. Res.* 4, 37–41. <https://doi.org/10.5194/asr-4-37-2010>.
- Stein, A.F., Draxler, R.R., Rolph, G.D., Stunder, B.J.B., Cohen, M.D., Ngan, F., 2015. NOAA's HYSPLIT atmospheric transport and dispersion modeling system. *Bull. Am. Meteorol. Soc.* 96, 2059–2077. <https://doi.org/10.1175/BAMS-D-14-00110.1>.
- Stohl, A., Seibert, P., Wotawa, G., Arnold, D., Burkhardt, J.F., Eckhardt, S., Tapia, C., Vargas, A., Yasunari, T.J., 2012. Xenon-133 and Caesium-137 releases into the atmosphere from the Fukushima Daiichi nuclear power plant: determination of the source term, atmospheric dispersion, and deposition. *Atmos. Chem. Phys.* 12, 2313–2343. <https://doi.org/10.5194/acp-12-2313-2012>.
- Sugiyama, G., Nasstrom, J., Pobanz, B., Foster, K., Simpson, M., Vogt, P., Aluzzi, F., Homann, S., 2012. Atmospheric dispersion modeling: challenges of the Fukushima Daiichi response. *Health Phys.* 102, 493–508. <https://doi.org/10.1097/HP.0b013e31824c7bc9>.
- Talerko, N., 2005. Mesoscale modeling of radioactive contamination formation in Ukraine caused by the Chernobyl accident. *J. Environ. Radioact.* 78 (3), 311–329. <https://doi.org/10.1016/j.jenvrad.2004.04.008>.
- Thompson, G., Field, P.R., Rasmussen, R.M., Hall, W.D., 2008. Explicit forecasts of winter precipitation using an improved bulk microphysics scheme. Part II: implementation of a new snow parameterization. *Mon. Weather Rev.* 136, 5095–5115. <https://doi.org/10.1175/2008MWR2387.1>.
- Voloshchuk, V.M., Shkvoets, O.Yu., 1993. Possible influence of meteorological conditions and changes aerosol source parameters on the spot structure formation of ground radioactive contamination. *J. Aerosol Sci.* 24 (1), 531.